



Since January 2020 Elsevier has created a COVID-19 resource centre with free information in English and Mandarin on the novel coronavirus COVID-19. The COVID-19 resource centre is hosted on Elsevier Connect, the company's public news and information website.

Elsevier hereby grants permission to make all its COVID-19-related research that is available on the COVID-19 resource centre - including this research content - immediately available in PubMed Central and other publicly funded repositories, such as the WHO COVID database with rights for unrestricted research re-use and analyses in any form or by any means with acknowledgement of the original source. These permissions are granted for free by Elsevier for as long as the COVID-19 resource centre remains active.



Development of a novel silver ions-nanosilver complementary composite as antimicrobial additive for powder coating

Jixing Cui^a, Yuanyuan Shao^a, Haiping Zhang^{a,*}, Hui Zhang^{a,b,*}, Jesse Zhu^{a,b}

^a Collaborative Innovation Center of Chemical Science and Engineering (Tianjin), School of Chemical Engineering and Technology, Tianjin University, Tianjin 300072, China

^b Department of Chemical and Biochemical Engineering, The University of Western Ontario, London, Ontario N6A 5B9, Canada

ARTICLE INFO

Keywords:

Antimicrobial additives
Powder coating
Silver nanoparticles
Encapsulation
 α -lipoic acid
Durability

ABSTRACT

Applying silver into coatings has become a prevalent method in fabricating antimicrobial surfaces. However, the concerns about durability always exist and limit its applications. Here, a highly inhibitory, active, durable, and easy-to-use silver ions-nanosilver antimicrobial additive for powder coatings was fabricated in this study. Silver nanoparticles were chemically bonded to the Ag, Cu, and Zn-ternary ion-exchanged zeolite by α -lipoic acid, which was then encapsulated by hydrophilic polymers. The fabricated silver ions and silver nanoparticles (Ag^+ -AgNPs) complementary structure provides a synergistic effect. Ag^+ is the main antimicrobial agent, while AgNPs act as a supplementary reservoir of Ag^+ . As well, the formed thin layer of silver nanoparticles and hydrophilic film prolongs the release of active Ag^+ from zeolite, and Ag^+ facilitates the activation of AgNPs. The results show that this additive indicates excellent antimicrobial activity to *E. coli*, *S. aureus*, *P. aeruginosa*, and *C. albicans*, and that the coatings with the additive exhibit over 99.99% reduction rate for the tested bacteria and fungi. The coating film is able to maintain over 99% antimicrobial reduction even after 1200 repeated solution wipings, or over 30 wash cycles of artificial sweat solution, indicating high durability. Furthermore, the yellowness of the coating is not evident ($\Delta b < 2$) despite the high loading of silver, and the silver nanoparticles have little impact on gloss, haze, and distinctness of the coating film image.

1. Introduction

Powder coatings have been widely used in many fields, including domestic appliances, automotive, building materials, transportation, and horticultural facilities, and are gradually replacing conventional liquid coatings [1,2]. Solvents are absent in powder coating, so the emission of VOCs is nil. As the emerging market of powder coating continues to grow, many functionalized powder coating applications have risen, including hydrophobic/hydrophilic [3], weathering resistant [4], high-temperature resistant [5], anticorrosive [6,7], self-healing [8] and antimicrobial coatings [9]. With the increase in living standards, people pay more attention to their health status and hygiene conditions. Pathogens can often exist on inanimate surfaces for hours, days, weeks or even longer. For example, the novel coronavirus COVID-19 has a half-life of 18 hrs at a temperature of 21–24 °C, with a relative humidity of 20% on a surface [10]. An investigation exhibits that the average number of microorganisms in rural areas is 138 CFU/cm² in China, while in urban areas it is 72 CFU/cm², and in public areas it is even

higher [11]. In order to avoid the spread of infectious diseases, the antimicrobial coating has become an important direction for development.

As antimicrobial functional additives to coatings, inorganic biocides gradually replace organic ones and become a dominant trend. Silver has been widely used for constructing antimicrobial coatings because of their broad-spectrum antimicrobial properties. The additives are primarily silver-containing materials loading on supporting carriers, e.g. zeolite, glass, ceramic, or zirconium phosphate complexes [12–15], where silver was generally in the ionic state. As a Lewis acid, Ag^+ has a high affinity to react with electron-donating groups, like phosphorous and sulfur-containing biomolecules on cell membranes and enzymes [16–18].

As a release-based antibacterial agent, silver-containing materials normally have the potential to release evident amounts of Ag^+ into solution. This property, on the other hand, will lead to the results that frequent wiping and cleaning of the surface of the antimicrobial coating will diminish the activity. It is reported that the silver is released up to

* Corresponding authors. Tel.: +1 519 6612111x81294 (Hui Zhang). Tel.: +86 15620090318 (Haiping Zhang).

E-mail addresses: hpzhang@tju.edu.cn (H. Zhang), hzhang1@uwo.ca (H. Zhang).

20–30% in the first washing [19]. Other contact liquid, e.g. sweat also aggravates the release. Von Goetz et al.[20] described that silver released more readily to form Ag-chloro complexes when treated with sweat, due to its high chloride content. An excessive amount of Ag^+ released from unprotected biocide additive is unnecessary and wasteful, because antimicrobial activity concentration can be as low as 10^{-7} g/L [21]. Therefore, a slow but smooth release of Ag^+ is preferable for longevity of the antimicrobial function. For this purpose, we have tried ternary ions-loading and polymer encapsulation to protect Ag^+ from reduction and lessen Ag^+ dissociation and diffusion [22,23]. These methods achieved a slow silver release rate and increased the durability of the antimicrobial coated surface. However, by merely controlling the ion dissociation and diffusion, the improvement is limited. Thus, developing a new mechanism providing a more controllable release of Ag^+ is of great significance for long-term antimicrobial activity.

Silver nanoparticles (AgNPs), another silver form, have also been widely studied as an antimicrobial agent [24,25] with nearly no toxic to the human cell, whose toxicity is much less than silver salts form at the equivalent mass loading of silver [26]. Considerable research efforts have shown that antimicrobial activity of AgNPs is related to silver ion release [27–30]. When AgNPs encounter water and oxygen, Ag^+ are

released from the surface of nanoparticles immediately. The release rate depends on nanoparticle size, shape, surface chemistry, temperature, oxygen concentration and light. Normally, the conversion rate from AgNPs to Ag^+ is limited, with first-order rate constant k , 4.1 day^{-1} for 4.8 nm AgNPs and 0.74 day^{-1} for 60 nm AgNPs [29]. This slow but sustainable release property is beneficial to increase the durability of antimicrobial additives for powder coatings.

In recent years, many studies concentrate on antimicrobial coatings of AgNPs, but most of them are not suitable for powder coatings. The formation of AgNPs coatings normally include surface polymerization [31], sol-gel [32], successive ionic layer adsorption and reaction (SILAR)[33], chemical vapor deposition (CVD)[34] and electrochemical deposition [35]. All of these methods need complicated coating processes and special modifications. For conventional powder coatings, the most convenient way is incorporating additives into the coating matrix. Currently, most of the additives are based on ion-form silver and the use of AgNPs to control silver release and improve the antimicrobial durability is seldom reported.

Nanoparticles employed in organic coatings, which are always less hydrophilic, have limited activity. Moist is hard to penetrate into the powder coatings matrix, so that the formation of Ag^+ from AgNPs is

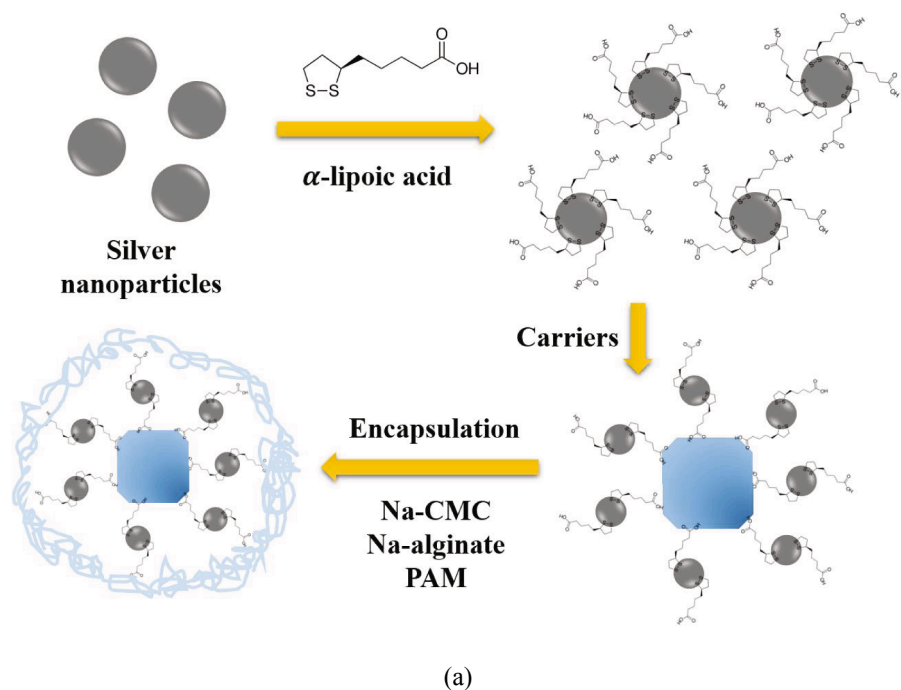


Fig. 1. Schematic illustration of (a) procedures of preparing antimicrobial additive by using lipoic acid as a crosslinker, and carriers used here were Linder type A (LTA) zeolite and Ag, Cu, Zn ternary ion-exchanged zeolite; (b) mechanism of Ag^+ release and antimicrobial activity.

inhibited due to the lack of enough chemical potential. Thus, a special structure providing a water micro-environment is needed. Also, unlike electrostatic interactions between Ag^+ and zeolite carrier, silver nanoparticles bind to zeolite by weak Van der Waal force and AgNPs can easily be leached out. The binding force between hydrophilic materials and zeolite is weak as well, and it is also a challenge to form a firm encapsulation.

To overcome the bottleneck of AgNPs additives, in the present study, a novel antimicrobial additive was prepared with a schematic procedure illustrated in Fig. 1(a) and the surface antimicrobial mechanism is described in Fig. 1(b). AgNPs and their carriers are encapsulated by hydrophilic materials. Incorporation of these nanoparticles into the hydrophilic polymeric environment enables them in contact with moisture and dissolved oxygen more easily. Furthermore, the polymer barrier can also provide a simple yet effective way to control the dispersion of Ag^+ [36–38]. Also, in order to reduce the leaching of AgNPs, the individual nanoparticle is modified by α -lipoic acid, which can anchor these silver nanoparticles tightly on the surface of the carrier, and the carrier used here is Ag, Cu, Zn ion-exchanged zeolite. Moreover, a comprehensive analysis on the structure, morphology, antimicrobial activity was conducted to illustrate the function of α -lipoic acid, encapsulation and synergistic effect of Ag^+ and AgNPs. The coatings with this additive inhibit the growth of several microbes, and show long-term effectiveness with low changes of visual appearance. The additive developed in this study can be used in uncountable types of products such as appliances, surfaces in public passenger vehicles, personal electronics, door handles, trolleys, elevators and so on, to prevent the spreading of disease.

2. Materials and methods

2.1. Materials

Commercial silver nanoparticles were purchased from Tanfeng Graphene Corp., China. Ion-exchanged zeolites were lab-made, with detailed descriptions available in previous work [22]. α -lipoic acid, carboxymethyl cellulose-Na (Na-CMC), alginate-Na were from Aladdin Co., Ltd., Shanghai, China. Polyvinylpyrrolidone (PVP) and Sodium dodecyl sulfate (SDS) were purchased from J&K Scientific Co., Ltd., China. DI water was used throughout the experiment. Commercial antimicrobial additive Zeomic AJ10N/D was from Zeomic Co., Ltd., Japan and Microkiller SRT-104 was from Ishizuka Co., Ltd, Japan.

Polyester powder coatings were from Huajiang Powder Technology Co., Ltd., Guangdong, China, whose composition and properties are listed in Table 1.

E. coli, ATCC25922, *S. aureus*, CMCC(B)26003, *P. aeruginosa*, CMCC (B)-10104, and *C. albicans*, CMCC(F)-98001, were obtained from Luwei Technology Co., Ltd., Shanghai, China.

Coating substrates used are aluminum plates of 0.5 mm thick \times 60 mm wide \times 75 mm long; T12G black and white metopac (metal) panels of 0.5 mm thick \times 76 mm wide \times 132 mm long, Leneta Co., Ltd., USA.

Table 1
Commercial powder coating specifications.

Class	Sub Class	Name	Components (wt%)
Binder	Resin	Polyester	91.79
	Curing Agent	TGIC	6.91
Additives	Flow Agent	P10	1.00
	Degassing	BEN	0.30
Density	1150 kg/m ³		
Gloss	High-glossy		
Surface appearance	Smooth		
Cure parameters	200 °C/10 min		
Pigment	Fluorescent orange		

2.2. Preparation of antimicrobial additives

Commercial silver nanoparticles (AgNPs, 30–50 nm) were firstly modified by α -lipoic acid (LA). Briefly, 0.1 g, 0.02 g, 0.01 g, 0.002 g of AgNPs were suspended in 100 mL deionized water by ultra-sonication for 30 min, and then under vigorous stirring, 30 mL 10^{-3} mol/L LA solution was added dropwise into AgNPs suspension, with continuous agitation for 30 min at 60 °C. LA solution was kept at 80 °C to obtain a clarified solution. Ag-Cu-Zn-Z (prepared from [22]) and LTA zeolite were used as carriers for AgNPs. 2 g of these carriers were respectively dispersed into deionized water and mixed with as-prepared AgNPs, with continuous stirring for 2hrs at 60 °C, pH 5.5–6.5.

Polymers used for encapsulation were polyacrylamide (PAM, 1%), sodium alginate (Na-alginate, 3%), sodium carboxy methylcellulose (Na-CMC, 7%). These three polymers were mixed with water at 80 °C by constant stirring until dissolved completely, then the as-prepared suspension of zeolite containing silver nanoparticles was added into the polymer mixture. This final mixture was stirred at 40 °C until it became a thick slurry. This slurry was spread on a flat surface in a fume hood for completely dry, preferably in a dark place. The compositions and description of prepared and commercial additives are listed in Table 2.

2.3. Preparation of antimicrobial coatings

Polyester powder coating ($D_{50} < 45\mu$ m) was mixed with antimicrobial additives (2.0 wt%) and tightly bonded with additive particles using pressure bonding method in order to avoid the separation of additive when performing electronic spraying process.

The aluminum plates were rinsed with DI water and wiped with 75% ethanol to remove soil and oil stains on the surface. They were then hung inside the booth and grounded appropriately. A larger panel was set behind the sample panels to avoid powder coating covering their backside. T12G black and white standard panels were treated with the same way as above, in order to precisely test the discoloration.

A Nordson Surecoat corona spray gun (Nordson Corp, USA) was used to manually coat the prepared sample panels. The corona charge generator had constant settings for each spraying: 40 kV of operating

Table 2
Description and silver contents of commercial and prepared additives.

Additive No.	Samples	Ag^+ loading	AgNPs loading	Description
Additive 1	Zeomic AJ10N/D	2.5 wt%	–	Commercial source
Additive 2	Microkiller SRT-104	1.0 wt%	–	Commercial source
Additive 3	Ag-Cu-Zn-Z	8.3 wt%	–	Ag, Cu, Zn ternary ion-exchanged zeolite
Additive 4	Ag-Cu-Zn-Z-Encap	8.3 wt%	–	Ag-Cu-Zn-Z encapsulated by hydrophilic polymers
Additive 5	Z-AgNPs(1.0 wt %)-Encap	–	1.0 wt%	LTA and AgNPs encapsulated by hydrophilic polymers
Additive 6	Ag-Cu-Zn-Z-AgNPs(1.0 wt %)-Encap	8.3 wt%	1.0 wt%	Ag-Cu-Zn-Z and AgNPs encapsulated by hydrophilic polymers
Additive 7	Ag-Cu-Zn-Z-AgNPs(0.1 wt %)-Encap-LA	8.3 wt%	0.1 wt%	Ag-Cu-Zn-Z and AgNPs (0.1 wt%) encapsulated by hydrophilic polymers, bonding with LA
Additive 8	Ag-Cu-Zn-Z-AgNPs(0.5 wt %)-Encap-LA	8.3 wt%	0.5 wt%	Same as additive 7 with AgNPs(0.5 wt%)
Additive 9	Ag-Cu-Zn-Z-AgNPs(1.0 wt %)-Encap-LA	8.3 wt%	1.0 wt%	Same as additive 7 with AgNPs(1.0 wt%)
Additive 10	Ag-Cu-Zn-Z-AgNPs(2.0 wt %)-Encap-LA	8.3 wt%	2.0 wt%	Same as additive 7 with AgNPs(2.0 wt%)

voltage, 40 μ A of current. Substrates were located 40 cm from the spray gun. Only the front side of the substrate sheet was sprayed. Once the sample panels were sufficiently coated with antimicrobial powder paint, they were transferred to the convection oven (Wanrui Corp, Shanghai) for curing. All samples were hung inside and cured at 200 °C for 10 min, during which the deposited powder with additives was melted, leveled, and cured, producing a fully continuous coating film.

2.4. Characterization of the additives and the coating surface

Absorption spectra were recorded on a UV-visible spectrophotometer (Hach DR6000, 190–1100 nm) using a 1.0 cm path length quartz cuvette. ATR-FTIR was analyzed by Thermo Fisher Nicolet iS10, 10 scans over the range 4000–500 cm^{-1} . Zeta potential test was performed by Malvern Zetasizer Nano ZS instrument equipped with a He-Ne laser operating at 632.8 nm and a scattering detector at 173°. Differential scanning calorimetry (Mettler Toledo DSC 3 instrument) was performed at a heating rate of 10 °C/min interval from 25 to 300 °C under 50 mL/min air as a purge gas, to test the heat stability of additives and to understand the curing degree of powder coating. Scanning electron micrographs (SEM) were performed on a Thermo Fisher Phenom XL scanning microscope, equipped with energy dispersive X-Ray spectroscopy (EDX). Wettability of the coating surface was performed by an automatic dynamic contact angle goniometer JC2000D3M (Zhongyixun, Beijing, China). Visual appearance was conducted by the Rhopoint IQ (Rhopoint Instruments) and the WF32 colorimeter (Shanghai Jiabiao). The color analysis includes ΔE and Δb measurements. The total color change is

$$\Delta E = \sqrt{(\Delta L)^2 + \Delta a^2 + \Delta b^2} \quad (1)$$

where ΔL suggests brightness varying from black (0) to white (100), Δa changes from red (+) to green (−), and Δb changes from yellow (+) to blue (−). The impact test of coatings was conducted on a universal impact tester following ASTM D2794.

The curing is a complex crosslinking process, and previous work confirmed that the curing reaction started from 120 °C and continued until 230 °C [22]. Total heat released from the reaction (ΔH_T) from 110 °C to 230 °C can be achieved by DSC analysis. Samples were cured at various temperatures and times, and the exothermal value (ΔH_R) for each condition was recorded by DSC analysis, and then the degree of curing can be calculated as:

$$\text{Degree of curing} = (\Delta H_T - \Delta H_R) / \Delta H_T \quad (2)$$

2.5. Analysis of the antimicrobial effects

The antimicrobial activity of the additives was evaluated by the disc diffusion method, which could form inhibition zones for detection. Activity assay was conducted by *E. coli*, ATCC25922, *S. aureus*, CMCC(B) 26003, *P. aeruginosa*, CMCC(B)10104, and *C. albicans*, CMCC(F)98001. 0.5 mL microbial suspension with approximate cell density of 10^5 colony-forming unit (CFU) or spores/mL was added to Mueller Hinton agar and spread inoculum over the surface evenly. Aseptic paper discs (6 mm) were dipped into 1 g/L additives solution. After drying in a dark place, the discs were placed onto the prepared MH medium and incubated at 38 °C for 24 h. Then the inhibition halo was measured.

ASTM E2180-07 standard was adopted to characterize the antimicrobial activity of the coating. Briefly, microbial solutions (10^6 CFU/mL) were pipetted to the sample coatings, and the number of microorganisms was measured before and after inoculation. Each test was performed in triplicate. The reduction rate was calculated as follows:

$$\% \text{reduction} = \frac{X_0 - \bar{X}}{X_0} \times 100 \quad (3)$$

where X_0 stands for the number of organisms after the 6hr incubation period for the control coating and \bar{X} represents the mean value for that of sample coatings.

Antimicrobial durability tests were performed by using two methods: wiping and impregnation. For the wiping method, 2.5 g/L dish soap solution was made and used to wipe the coatings with a sponge. One cycle is defined as a 60-time back-and-forth wipe with a pressure of 20 kPa. The coating was cleaned with 50 mL water after wiping. The other method was impregnating the antimicrobial coatings into 0.2 wt% dish soap, artificial sweat, and LB broth, respectively, and then continuously agitating them for 2 hrs. The abovementioned steps are set as one cycle. According to EN1811-1999 standard, artificial sweat has a composition of 1.08(w/v) % NaCl, 0.12(w/v) % lactic acid and 0.13(w/v) % urea. After each cycle, antimicrobial activity measurement was performed. Leaching test was performed by immersing the coatings to 0.9 wt% NaNO_3 solutions for 6hrs, and the leaching Ag^+ were tested by ICP-MS (Thermo iCAP RQ). The leaching test was performed on the newly-made coatings and coatings after 10 wash cycles.

3. Results and discussion

3.1. Characterization of antimicrobial additives

3.1.1. UV-vis analysis of the dispersed AgNPs

Commercial silver nanoparticles are usually dispersed in an aqueous solution before applications, and ultrasonic dispersion is the common method. PVP, SDS and LA are commonly used capping agents for effectively dispersing silver nanoparticles. In order to select appropriate AgNPs for further treatment, AgNPs with these three common capping agents (sodium dodecyl sulfonate, SDS; polyvinylpyrrolidone, PVP; α -lipoic acid, LA) were tested to compare with the pure AgNPs. Fig. 2 shows the UV-visible spectra of the dispersed silver nanoparticles. The absorption peak is caused by surface plasmon resonance, while the position of the extinction peak represents the size of AgNPs and the width of FWHM (full width at half maximum) determines the polydispersity [39,40]. According to Fig. 2, the size of AgNPs is in the rank of AgNPs-PVP < pure AgNPs < AgNPs-SDS < AgNPs-LA and the polydispersity is in a series of AgNPs-PVP < AgNPs-SDS < pure AgNPs < AgNPs-LA. AgNPs-PVP suspension has the best dispersion, while AgNPs-SDS exhibit a slightly larger particle size. The reason is that the isoelectric point of AgNPs (without treatment) corresponds to pH in a range of 1.5–3.5 [41]. Thus, negatively charged silver nanoparticles are achieved because the

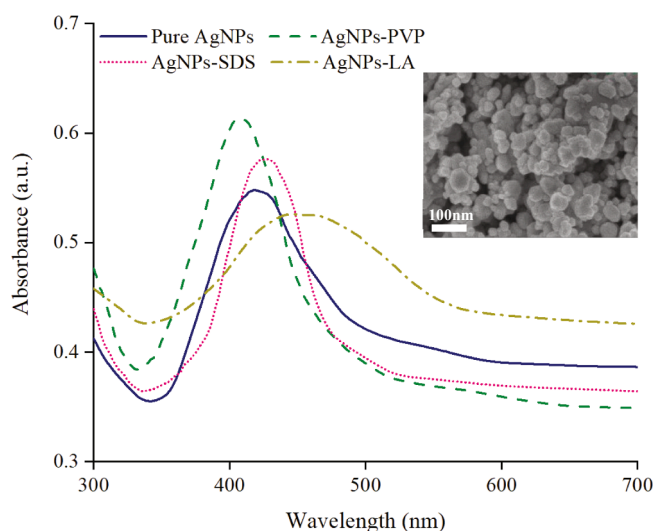


Fig. 2. UV-vis absorption spectra of AgNPs with different capping agents suspended in DI water. Inset: SEM graph of pure AgNPs.

suspension has a pH of 6.5. SDS, as an anion capping agent, cannot appropriately cover the AgNPs surface. Comparing AgNPs-PVP and AgNPs-SDS, AgNPs suspension with LA display larger particle size and broader size distribution. This is probably because the firm and rapid bonding between AgNPs and LA impedes further decreasing the size of the AgNPs cluster. By contrast, pure AgNPs provide a better dispersion than AgNPs-LA, and their clear surface is readily to be modified with α -lipoic acid. Accordingly, AgNPs are firstly dispersed in water and then functionalized with LA in the following process.

3.1.2. FTIR analysis of additives

Fig. 3 exhibits the FTIR spectra comparison of α -lipoic acid and lipoic acid-functionalized AgNPs. As pure α -lipoic acid, the characteristic absorption peak of the stretching vibration of the carbonyl group (C=O) is 1694 cm^{-1} while the band at 2930 cm^{-1} corresponds to C-H strong stretching vibration, and the band at 734 cm^{-1} is in line with S-S weak stretching vibration [42,43]. By contrast, for lipoic acid-functionalized AgNPs, the band at 734 cm^{-1} disappears, which indicates the breakage of disulfide bonds (S-S). It is expected that under the alkaline or heating conditions, disulfide deprotonates and forms a pseudo covalent bond with silver (Ag-S). It is important to mention that zeta-potential of silver nanoparticles' colloids without LA is -45 mV when $\text{pH} = 6.5$, while AgNPs-LA suggests a value of -23 mV at the same pH. Therefore, the addition of LA change the surface of AgNPs, and these carboxyl-end AgNPs enhance the negative charge of the particles, reducing the agglomeration.

Fig. 4 indicates the FTIR spectra comparison of pure zeolite, Ag-Cu-Zn-Z-Encap, and Ag-Cu-Zn-Z-AgNPs (1.0 wt%)-Encap-LA. The broad-band at 3338 cm^{-1} and weak peak band at 1651 cm^{-1} correspond to O-H stretching and $\delta(\text{H-O-H})$ bending vibration for water molecules in the hydrated samples [44]. The noticeable band at 961 cm^{-1} represents asymmetric stretching vibration of $\delta(\text{Si-O})$, where Si-O (bridging) and Si-O (non-bridging) bonds are overlapped, while symmetric $\delta(\text{O-Si-O})$ stretching band is at 667 cm^{-1} [44,45]. The weak band at 1419 cm^{-1} is newly formed in encapsulated zeolites and the peak at 1651 cm^{-1} shows an enhancement, which indicates the asymmetric and symmetric stretching vibration of carboxylate $\delta(\text{COO}^-)$ [46,47]. This is produced by the carboxyl groups in Na-CMC and Na-alginate hydrophilic polymers. The band at 1740 cm^{-1} corresponds to aliphatic C=O stretching that only appears on Ag-Cu-Zn-Z-AgNPs (1.0 wt%)-Encap-LA and indicates the formation of an ester bond between the carboxyl and hydroxy

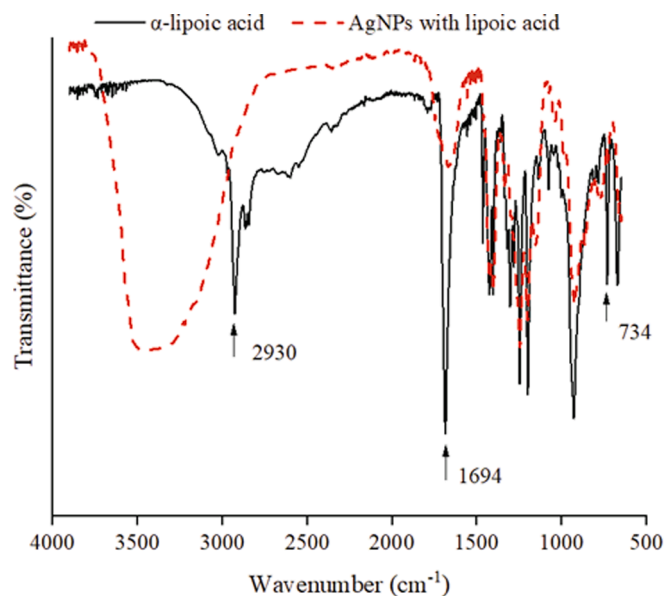


Fig. 3. FTIR spectra ($500\text{--}4000\text{ cm}^{-1}$) of α -lipoic acid-functionalized AgNPs in comparison with pure lipoic acid.

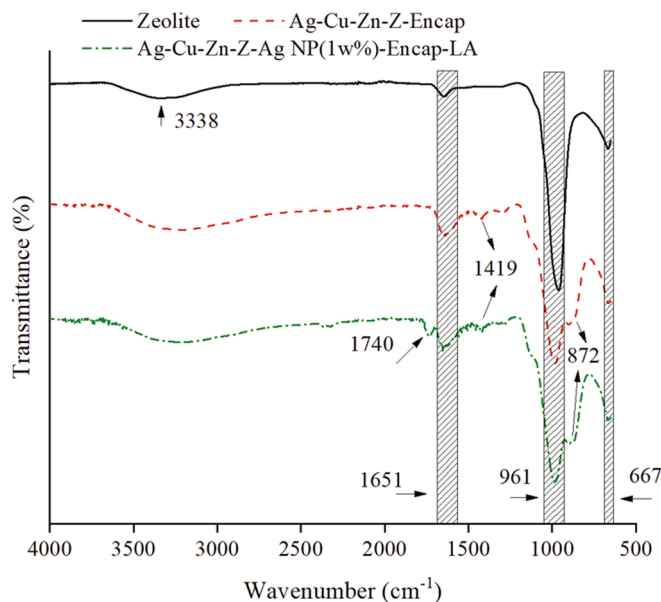


Fig. 4. FTIR spectra ($500\text{--}4000\text{ cm}^{-1}$) of Ag-Cu-Zn-Z-Encap and Ag-Cu-Zn-Z-AgNPs (1.0 wt%)-Encap-LA in comparison with pure zeolite (LTA).

functional groups. The carboxyl group exists on LA covered-AgNPs, and the hydroxyl group appears on both the surface of zeolite and hydrophilic polymers. The Cu-O stretching band at 872 cm^{-1} explains Cu^{2+} in zeolite binds with $-\text{OH}$ groups in hydrophilic polymers, and it is a complementary way to combine these two materials together [48].

3.1.3. DSC analysis of antimicrobial additives

The profile of DSC in Fig. 5 displays the changes in heat flow in several additives from $25\text{ }^\circ\text{C}$ to $300\text{ }^\circ\text{C}$. Zeolite is a stable aluminum silicate, and the structure will not change until $900\text{ }^\circ\text{C}$ [49]. Therefore, the change of heat flow rate within $300\text{ }^\circ\text{C}$ is mainly based on the dehydration and probable reaction of Ag^+ .

Hydrated zeolite includes hygroscopic and cation-hydrated water. Additives were dried primarily in an oven, therefore surface water on zeolite is absent. Endothermic peaks for pure zeolite, Ag-Cu-Zn-Z, Ag-Cu-Zn-Z-Encap, Ag-Cu-Zn-Z-AgNPs (1.0 wt%)-Encap, Ag-Cu-Zn-Z-AgNPs (0.5 wt%)-Encap-LA, Ag-Cu-Zn-Z-AgNPs (1.0 wt%)-Encap-LA and Ag-Cu-Zn-Z-AgNPs (2.0 wt%) - Encap-LA are at $179\text{ }^\circ\text{C}$, $173\text{ }^\circ\text{C}$, $182\text{ }^\circ\text{C}$, $181\text{ }^\circ\text{C}$, $188\text{ }^\circ\text{C}$, $189\text{ }^\circ\text{C}$ and $195\text{ }^\circ\text{C}$, respectively. Apparently, the

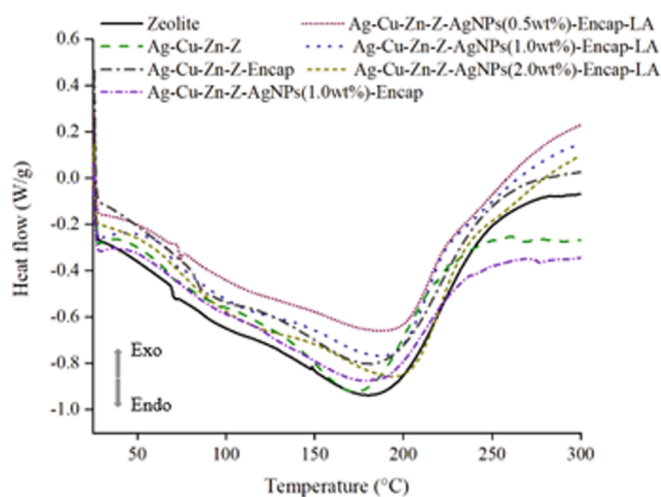


Fig. 5. DSC profiles of six Ag^+ or Ag^+ -Ag NP additives in comparison with pure zeolite (LTA).

peak for Ag-Cu-Zn-Z is found left-shifted. Due to the lack of protecting encapsulation, the reduction of ionic silver will take place at 170 °C –200 °C. This process is an exothermic reaction, and the released heat pushes the peak to lower temperatures. The hydrophilic polymer encapsulated ones have a film of protection, blocking water molecules escaping from inside. Thus, the dehydration of these additives will occur at a higher temperature. When introducing AgNPs, a higher dehydration temperature is observed, because the covered nanoparticles impede the departure of water from the zeolite. When increasing the amount of nano-silver, water molecules release is more difficult, and the temperature increases to 195 °C when adding 2 wt% nano-silver. Besides dehydration, the covered zeolite isolates Ag⁺ in zeolite from the outside, and zero state nano-silver covering outside, so the redox process lessens, and silver in its ionic state is protected [22]. As for Ag-Cu-Zn-Z-AgNPs (1.0 wt%)-Encap, due to the lack of LA, the covered film is imperfect, so most AgNPs cannot stay on the surface of zeolite, showing a similar dehydration peak (181 °C) with Ag-Cu-Zn-Z-Encap (182 °C). DSC analysis manifests that Ag⁺-AgNPs additive becomes more stable than Ag⁺ ones, because the covered polymers and AgNPs layer provides protection to Ag⁺ and allows them to withstand higher temperatures.

3.1.4. SEM analysis of additives

Images of Ag-Cu-Zn-Z, Ag-Cu-Zn-Z-Encap, Ag-Cu-Zn-Z-AgNPs (1.0 wt%)-Encap and Ag-Cu-Zn-Z-AgNPs (1.0 wt%)-Encap-LA additives are displayed in Fig. 6 (a), (b), (c) and (d), respectively. Ternary ion-exchange zeolites show the same morphology with pure zeolites, which are cubic blocks with a diameter of around 1–2 μm. Encapsulated zeolites shown in (b) reveal encapsulated zeolite particles, but the covered film is incomplete and there are many holes and breakages present. The thickness of the film is various, and some thin film is observed. The hydrophilic polymer covered the zeolite through the interaction with copper ions and OH groups. However, this combination is unstable due to the weak electrostatic force between them. Fig. 6 (c) and (d) perform the morphology of Ag-Cu-Zn-Z-AgNPs (1.0 wt%)-Encap (c) and Ag-Cu-Zn-Z-AgNPs (1.0 wt%)-Encap-LA (d) additives. It can be found that compared to (c), the surface of the zeolite in (d) is covered with a thicker film, and the original appearance of zeolite is hidden. The size of individual antimicrobial particles increases by about 0.2–0.3 μm. Their enlarged images are shown in Fig. 6 (e) and (f). Without the lipoic acid, the breakage of the film appears, and silver nanoparticles are exposed to the outside. Silver nanoparticles adhere to zeolite by weak Van der Waals force, so the nanoparticles may fall off when grinding and sieving. Additives with LA are well-covered particles, which contain nano-silver inside the hydrophilic polymer. The encapsulated nano-silver binds tightly to the zeolite and cannot depart from additive particles. EDX in Fig. 6 (g) and (h) confirm the results. Higher content of silver (2.16 wt%) is observed in LA-absent additive, while (h) presents little silver (0.09 wt%) outside the additive particle. Moreover, the amount of sodium element in the LA-contained additive is higher, representing the covered hydrophilic polymers (Na-CMC and Na-alginate).

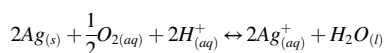
The function of LA can be further illustrated from Fig. 7, which displays the backscattered electrons (BSEs) SEM image of Ag-Cu-Zn-Z-AgNPs (1.0 wt%)-Encap and Ag-Cu-Zn-Z-AgNPs (1.0 wt%)-Encap-LA. Brighter parts indicate the silver elements due to its high atomic number. AgNPs fall off from zeolite particles and the scattered nanoparticles agglomerate into clusters. These agglomerations of silver nanoparticles lose antimicrobial effect, resulting in a decrease of effective silver. Moreover, the clusters dispersed in powder coatings, which will form black or grey spots on the coating surface, seriously affect the visual appearance. Also, some nanoparticles adhere to the outer surface of the hydrophilic polymer, which are still easily dropped out in the follow-up process. With the help of α-lipoic acid, the silver nanoparticles are wrapped inside the hydrophilic polymer and immobilized on the zeolite, and silver is seldom observed outside zeolite. EDX elemental analyses (c) and (d) confirm that the brighter parts clinging to the polymer surface are nano-silver. The content of silver in the LA-containing sample is

lower than that in LA-absent ones. Though small parts of nano-silver were not encapsulated inside, they chemically bond to the hydrophilic polymer, and these strong bonds suppress AgNPs from leaching out even with severe treatment. Fig. 7 (e) verifies that the formed clusters outside the carrier are mainly silver element (white circle in Fig. 7 (b)).

3.1.5. Antimicrobial activities of the additives

In this study, the inhibitory effect of antimicrobial additives is performed by the Kirby-Bauer disc diffusion method. The diameter of inhibition rings was measured and shown in Fig. 8. Seen from Fig. 8, both Ag⁺ and Ag⁺-AgNPs antimicrobial additives show excellent antimicrobial activity against *E. coli* and *S. aureus*. An inhibitory effect on *E. coli* is superior to that of *S. aureus*, which is due to the thicker peptidoglycan layer of *S. aureus* as gram-positive bacteria. Commercial additives show low effectiveness owing to the low silver content (Zeomic 2.5 wt%, Microkiller 1.0 wt%). Additives 3 and 4, which do not contain nano-silver, show good inhibitory effects, but the encapsulated one decreases slightly. It can be inferred that the encapsulated material inhibits the release of Ag⁺. Therefore, the inhibited Ag⁺ is protected, and can last for a longer time.

When introducing AgNPs, antimicrobial activity remains. AgNPs can convert to Ag⁺ by the following reaction,



AgNPs can serve as a reservoir and provide Ag⁺ continuously. Liu et al [27] indicate that dissolved oxygen with protons can produce peroxide intermediates, which is able to rapidly oxidize Ag⁰ to Ag⁺. In contrast to additives 4 and 9, AgNPs-containing encapsulated additives have a better inhibitory effect than the AgNPs-absent ones, which indicates the outer layer of AgNPs would form Ag⁺ to make the supplement. On the other hand, additive 5 (Z-AgNPs-Encap) shows poor effectiveness, because AgNPs oxidation rate is slow, with a first-order rate constant $k = 0.74 \text{ day}^{-1}$ for 60 nm AgNPs [29]. Therefore, it will take a long time to accumulate Ag⁺ to the minimum inhibitory concentration, and in order to improve the immediate antimicrobial activity, original Ag⁺ are necessary. Comparing additive 6 and 9, although both of them have the same Ag⁺ and AgNPs loading, additive 9 exhibits a higher inhibitory effect due to more bonding of AgNPs by LA. In contrast to additives 7–10, with the increase of the amount of nano-silver, the antimicrobial activity increases but goes down when an even higher amount of silver (2%) is included. The superabundant nano-silver forms a thick layer on zeolite, which could impede ion-exchange activity.

The prepared additives have a similar inhibitory effect on other kinds of microorganisms. Fig. 9 displays the antimicrobial activity of additive Ag-Cu-Zn-Z, Ag-Cu-Zn-Z-Encap, and Ag-Cu-Zn-Z-AgNPs (1.0 wt%)-Encap-LA. The additives provide an inhibitory effect on *E. coli* (gram-negative), *S. aureus* (gram-positive), *P. aeruginosa* (gram-negative), and *C. albicans* (yeast). All additives show a strong inhibition on *P. aeruginosa*, despite its multidrug-resistant feature. A weak effect is observed on yeast microorganisms, because the cell has a nucleus, which can effectively protect DNA from being damaged by Ag⁺.

3.2. Characterization of the antimicrobial coating surface

3.2.1. SEM analysis of coatings surface

Traditional powder coating production includes the following processes, i.e. pre-mix → extrusion → colling & chipping → grinding, classifying & screening → electrostatic spraying. Additives can be incorporated before or after extrusion. Under most circumstances, the pre-extrusion method deteriorates the coating surface ascribing to Ag⁺ reduction. The post-extrusion method can avoid this and the pressure bonding method is used to fasten additive and coatings together. Fig. 10 presents the morphology of the coating surface which indicates several additive particles are in close proximity to the surface. For the whole

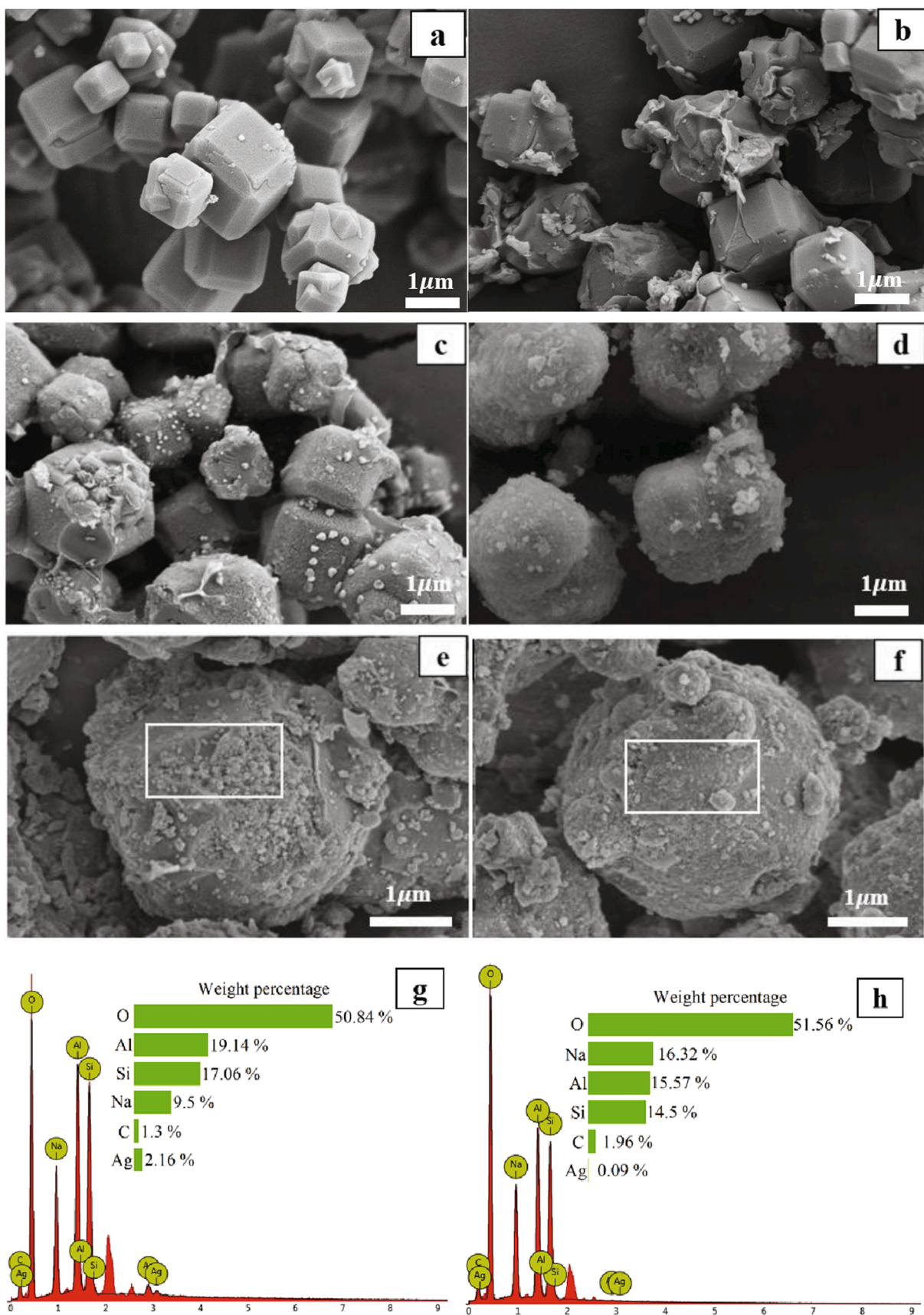


Fig. 6. Images of (a) LTA, (b) Ag-Cu-Zn-Z-Encap, (c) Ag-Cu-Zn-Z-AgNPs (1.0 wt%) -Encap and (d) Ag-Cu-Zn-Z-AgNPs (1.0 wt%) -Encap-LA, taken on SEM micrographs. (e) and (f) indicate the enlarged images of Ag-Cu-Zn-Z-AgNPs (1.0 wt%) -Encap and Ag-Cu-Zn-Z-AgNPs (1.0 wt%) -Encap-LA. (g) and (h) present EDX mapping test for the marked surface areas of (e) and (f) respectively.

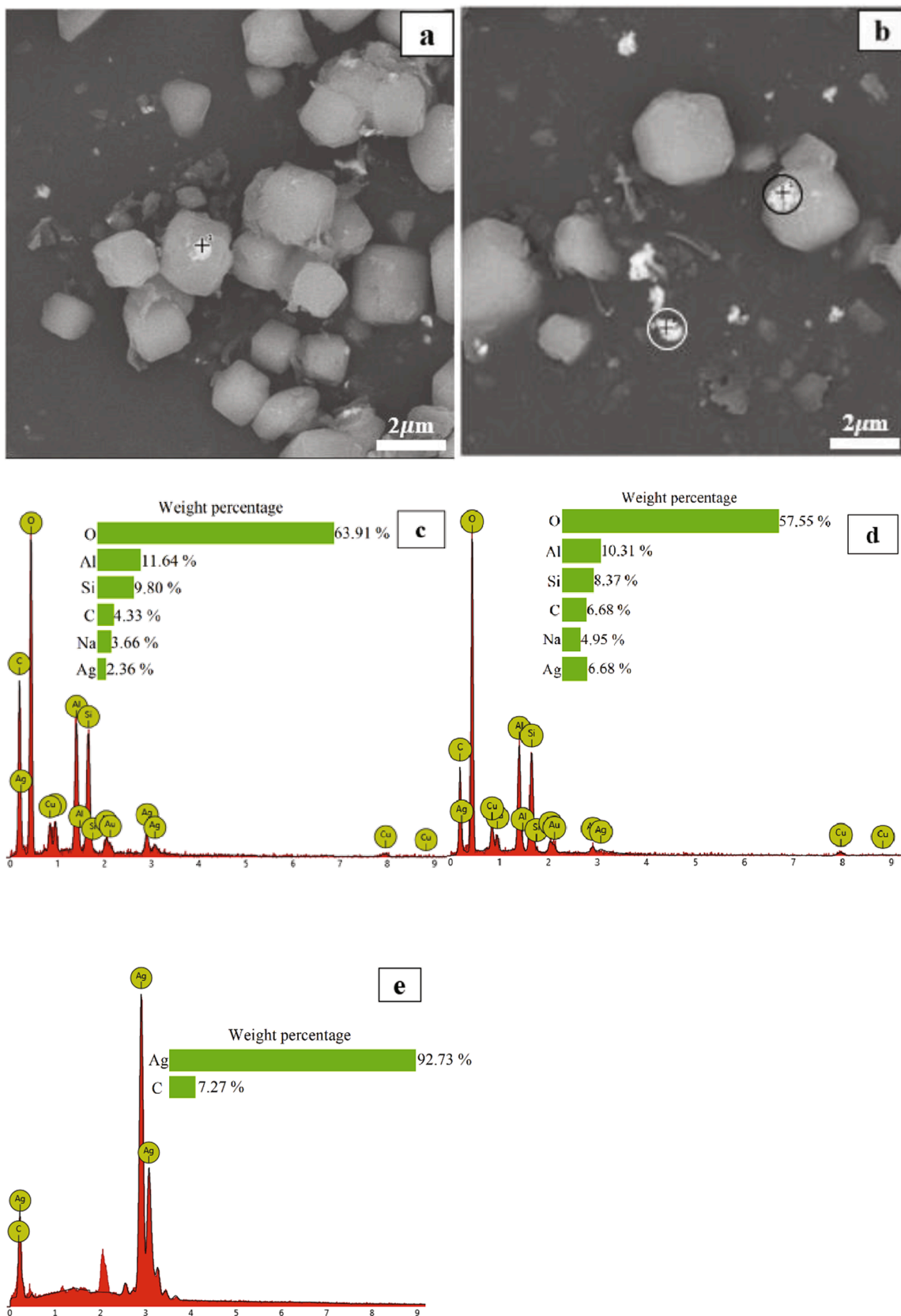


Fig. 7. Images of (a) Ag-Cu-Zn-Z-AgNPs (1.0 wt%)-Encap-LA, (b) Ag-Cu-Zn-Z-AgNPs (1.0 wt%)-Encap are taken on backscattered electrons SEM imaging. And (c) illustrates elements analysis of Ag-Cu-Zn-Z-AgNPs-Encap in the position of black cross of (a), while (d) and (e) indicate elements analysis of Ag-Cu-Zn-Z-AgNPs (1.0 wt%)-Encap-LA, in the position of black circle and white circle of (b) respectively.

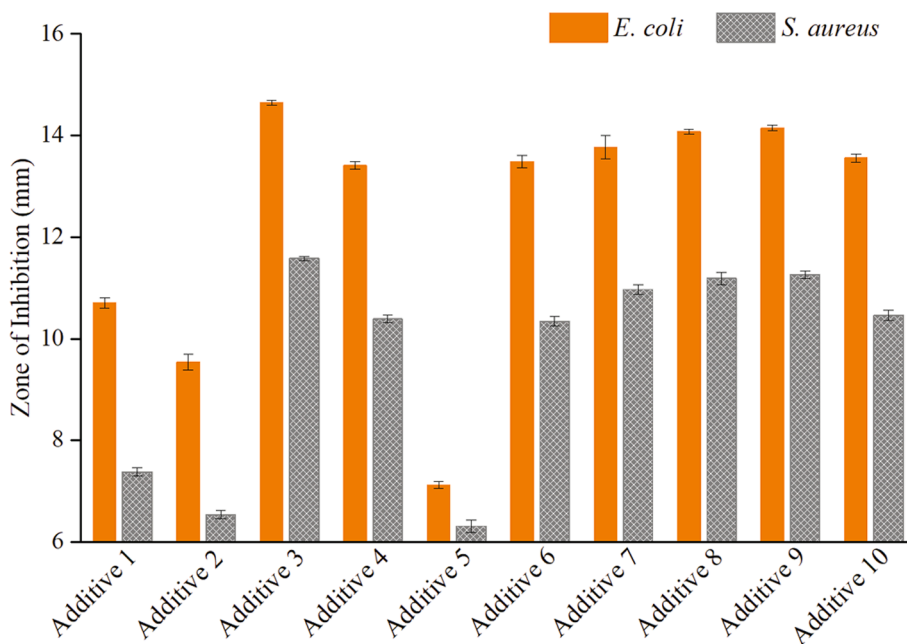


Fig. 8. Comparison of inhibition zone of ten additives against *E. coli* and *S. aureus*.

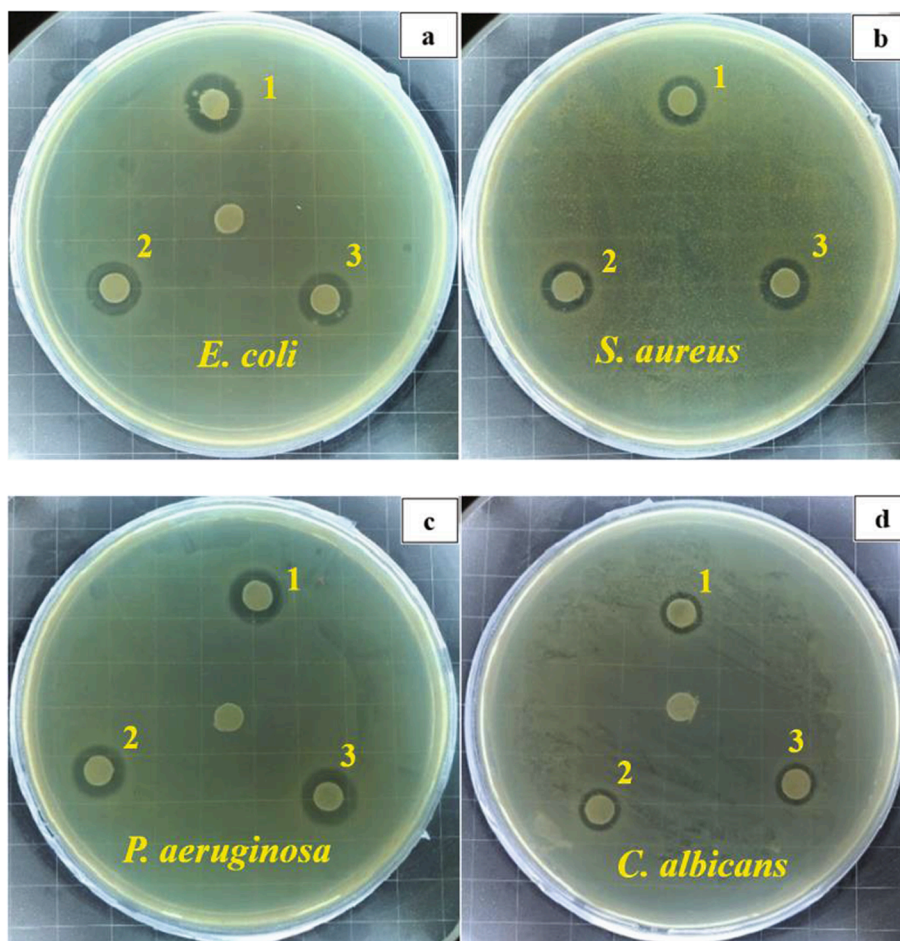


Fig. 9. Images of inhibition halo of three antimicrobial additives against *E. coli* (a), *S. aureus* (b), *P. aeruginosa* (c), and *C. albicans* (d), 1, Ag-Cu-Zn-Z; 2, Ag-Cu-Zn-Z-Encap; 3, Ag-Cu-Zn-Z-AgNPs (1.0 wt%)-Encap-LA.

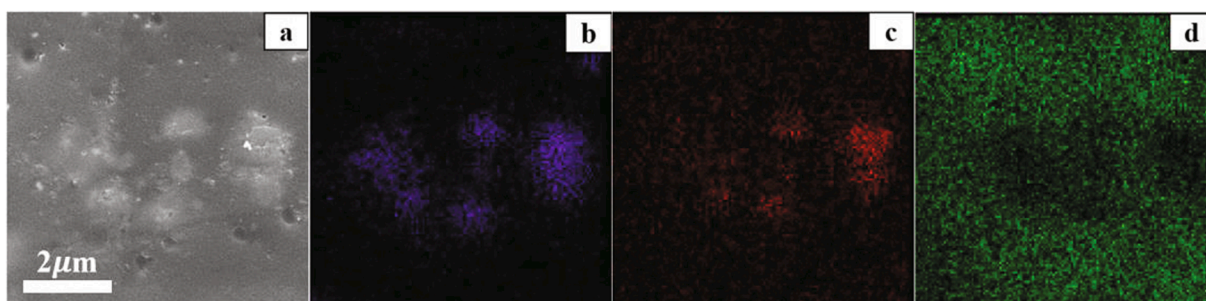


Fig. 10. SEM images of (a) antimicrobial powder coating surface and EDX elements analysis for (b) aluminum, (c) silicon, and (d) carbon. Additive: Ag-Cu-Zn-Z-AgNPs (1.0 wt%)-Encap-LA.

coating, a large number of additive particles spread on this surface with a density of 6×10^7 particles/cm², correspondent to 23.4 μg/cm² of silver loading, below the cytotoxicity threshold according to literature [50]. The obtained results by EDX analysis also enclose the additive particles embedded on the surface. The signal of aluminum and silicon from Fig. 10 (b) and (c) suggests the distribution of additive because aluminum and silicon are main composition of zeolite, while the even distribution of carbon from Fig. 10 (d) represents the dispersion of polyester coating, and areas around zeolite show a little darker due to the relatively low carbon content of additive.

3.2.2. Antimicrobial activity

The standard ASTM E2180-07 was adopted for the antimicrobial test of the coatings, and the initial *E. coli* concentration remained consistent. Commercial sources Zeomic AJ10N/D and Microkiller SRT-104 were performed as well, and the control coating was coated with polyester powder coating without additive. Fig. 11 shows the change of the number of *E. coli* in antimicrobial coatings within 6 hrs. The thickness of the coating films was maintained at 55 – 65 μm.

As can be seen from Fig. 11, the number of bacteria in the control coating increased by 2 orders of magnitude within 6 hrs. Bacteria in Z-AgNPs (1.0 wt%)-Encap additive coating also outnumbered the initial value, but was still better than the control coating, with a reduction rate of 71.6%. The two commercial additives decrease the number of bacteria with reductions of 94.93% (Zeomic) and 93.92% (Microkiller), respectively. The two commercial sources contain low silver content, so many vacancies exist on the zeolite carrier, and these vacancies are not utilized properly, leading to weak silver releasing ability. Other additives exhibit excellent antimicrobial properties, and all of them have a higher silver loading of at least 8.3 wt%. The numbers of bacteria reduce

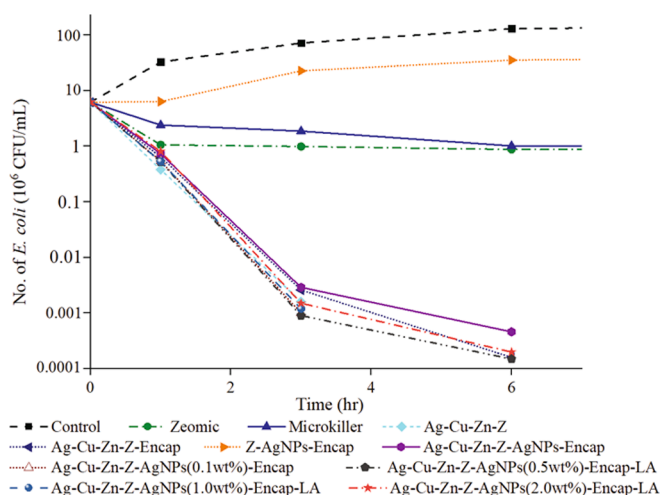


Fig. 11. Antimicrobial activity of powder coating surfaces with ten additives against *E. coli*. Test method: ASTM E2180-07.

by 4–5 orders of magnitude in 6 hrs, and the reduction rate reached over 99.99%. Moreover, for Ag-Cu-Zn-Z, Ag-Cu-Zn-Z-Encap and Ag-Cu-Zn-Z-AgNPs (1.0 wt%)-Encap-LA coatings, no *E. coli* was detected at 6 hrs. Among the additives, Ag-Cu-Zn-Z has the lowest number of *E. coli* at the 1 hr test, indicating high antimicrobial activity. This is because the release of Ag⁺ in this additive is rapid and abundant, but the excessive release of Ag⁺ is unfavorable to the durability. Although the initial antimicrobial efficiencies of the fabricated additives from this test are revealed informative, the longevities of them are to be determined from different accelerated assessments.

3.2.3. Durability of antimicrobial activity

The antimicrobial additive in the coating will be subject to loss of numerous Ag⁺ after each washing and wiping treatment, making the surface gradually lose the antimicrobial activity. Fig. 12 performs the changes in the reduction rate for seven additives after different wash cycles. The reduction rate of Ag⁺ additive Ag-Cu-Zn-Z gets down to under 99% after 12 cycles. Once encapsulated, Ag-Cu-Zn-Z-Encap increases to 15 washing cycles (900 wipings) because the polymer barrier suppresses the silver ion release. Furthermore, when introducing AgNPs, durability remarkably increases, i.e. for Ag-Cu-Zn-Z-AgNPs (1.0 wt%)-Encap to 16 cycles, for Ag-Cu-Zn-Z-AgNPs (0.1 wt%)-Encap-LA to 15 cycles, for Ag-Cu-Zn-Z-AgNPs (0.5 wt%)-Encap-LA to 17 cycles, for Ag-Cu-Zn-Z-AgNPs (0.1 wt%)-Encap-LA to 20 cycles and for Ag-Cu-Zn-Z-AgNPs (2.0 wt%)-Encap-LA to 20 cycles. The covered additive by AgNPs layer can slow down the Ag⁺ release rate from zeolite and provide extra Ag⁺, which could decrease the consumption of silver and prolong antimicrobial activity. Moreover, the synergistic action of Ag⁺ and AgNPs cannot be neglected, both of which experience a mutually

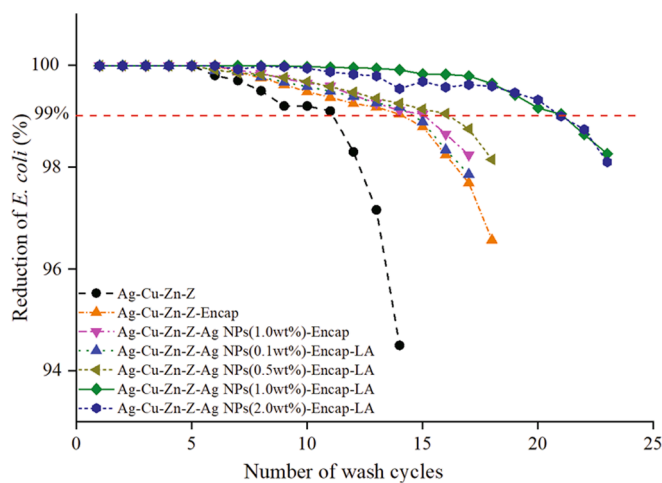


Fig. 12. Antimicrobial activity of seven Ag⁺ or Ag⁺-AgNPs additives after several wash cycles against *E. coli*. Additives which contain AgNPs could endure more wash cycles.

interacting process. When performing the ion-exchange procedure, surrounding ions pass through the encapsulation layer, bringing water and dissolved oxygen, and stimulating the oxidization of nano-silver. Moreover, some of the Ag^+ oxidized from nano-silver were adhere to its surface rather than released to the environment, so the surrounding ions could replace the adhering ions to prompt release. Also, the ion-exchange process makes ions frequently move in and out of the AgNPs layer, promoting the update of surface Ag^+ . When comparing Ag-Cu-Zn-Z-AgNPs (1.0 wt%)-Encap and Ag-Cu-Zn-Z-AgNPs (1.0 wt%)-Encap-LA, the latter endures 5 more cycles than the former, which again confirms the superiority of lipoic acid. The leaching-out silver nanoparticles will lose their antimicrobial activity due to agglomeration. With the increase of AgNPs addition, more washing cycles are achieved. Ag-Cu-Zn-Z-AgNPs (1.0 wt%)-Encap-LA and Ag-Cu-Zn-Z-AgNPs (2.0 wt%)-Encap-LA can endure 20 wash cycles (1200 wipings), indicating silver nanoparticles successfully works as a reservoir for Ag^+ . However, an extra increased amount of nano-silver has no benefit to durability. This is because if Ag^+ in zeolite is consumed up, the overdose addition of AgNPs are worthless, thus the antimicrobial activity largely decreases when losing synergistic and complementary action. Therefore, there is an optimal ratio between Ag^+ and AgNPs. According to experiment results, the preferable amount of AgNPs is 1.0 wt%, indicating the ratio of Ag^+ and AgNPs is 8.3:1.

Antimicrobial powder coating is generally applied to places where people frequently touch, such as handles and handrails in public transportation. Therefore, human sweat has a great influence on the durability of antimicrobial additives. Artificial sweat was used to simulate real sweat to determine the durability of antimicrobial coatings. However, the composition of sweat not only varies between individuals but also depends on the part of the body, age, season, infection status, and level of activity. There are several formulations of artificial sweat according to the AATCC Test Method 15–2002, British EN1811-1999, and ISO105-E04-2008E standards. Kulthong et al [51] investigated that silver was released at the highest level with the formulation EN1811-1999, thus EN1811-1999 was used as artificial sweat formulations, which contained lactic acid, urea, and NaCl. Ag-Cu-Zn-Z-AgNPs (1.0 wt%)-Encap-LA was selected as an additive and *E. coli* was set as the test strain. The other two contrast tests were 0.2 wt% dish soap solution and LB broth. Fig. 13 exhibits the inhibitory effect after 40 cleaning cycles, indicating that antimicrobial activity declines when the washing cycle increases, but all of them have no less than a 99% reduction rate after 30 cleaning cycles. Among them, artificial sweat shows the fastest declining rate, and is followed by dish soap solution. This is probably due to the high concentrations of NaCl in the artificial sweat (artificial sweat 19.9

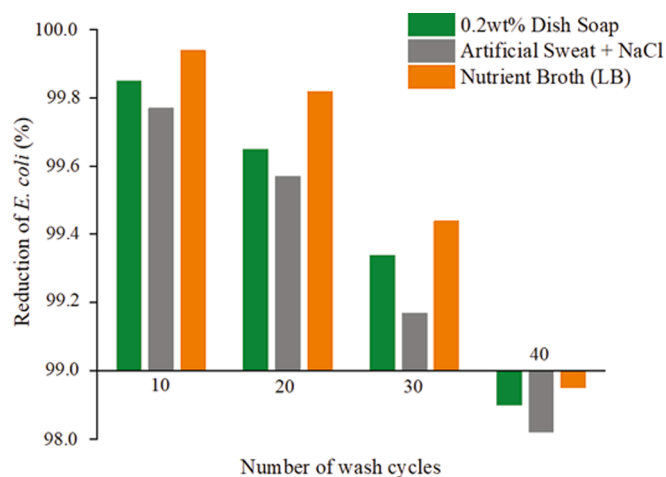


Fig. 13. Antimicrobial performance of Ag-Cu-Zn-Z-AgNPs (1.0 wt%)-Encap-LA after 40 wash cycles. 1 cycle equals to 2 hrs of continuous agitation in each of the solutions. Artificial sweat was made of lactic acid, urea, and NaCl.

g/L NaCl; LB broth 10 g/L NaCl), as the high concentration of Na^+ can accelerate the ion-exchange process. Moreover, the acidity can also be a significant contributing reason (i.e. artificial sweat pH = 6.5; LB broth pH = 7.5; dish soap pH = 7.8) because protons are one of the key materials during the silver nanoparticle oxidation process.

In conclusion, AgNPs-incorporated additives have much better durability than AgNPs-absent ones, especially for the ones containing LA. However, it is not the case that a higher amount of AgNPs translates to better durability. The effectiveness will be reduced when Ag^+ is consumed. The synergistic effect of AgNPs and Ag^+ is significant, and the existence of Ag^+ strongly accelerates the oxidation process. Furthermore, high salinity and low pH reduce durability.

3.2.4. Leaching

To further understand the release of ions on the coating surface, the leached silver is measured after immersing the coated surface into NaNO_3 solutions. Fig. 14 indicates the amount of Ag^+ release from five additive-incorporated coatings before and after wash cycles. The releasing amount of silver for Ag-Z after 10 wash cycles is low due to the fast ion-exchanged rate of Ag^+ with surrounding ions. While Ag-Cu-Zn-Z slows down the consumption of Ag^+ because the release of Zn^{2+} can partly compensate the release behavior of silver, prolonging the available time for silver. It is found that the additive encapsulated with hydrophilic materials, working like a protection shield, effectively reduce the consumption of Ag^+ during wash cycles. AgNPs-incorporated additive indicates a better slow-releasing effect of Ag^+ . The loss of silver during wash cycles is less, and the leached amount of silver after ten wash cycles is close to that of the newly-made coatings. However, without being modified by LA, silver consumption during washing is more severe comparing to LA-contained ones because such an amount of unanchored AgNPs are easily departing from carriers. AgNPs encapsulated inside hydrophilic polymer keep active and release Ag^+ slowly and constantly. Antimicrobial activities of these coatings are illustrated in Fig. 12, section 3.2.3, which proves a slow-releasing rate of Ag^+ achieves long durability. The concentration of leaching Ag^+ in solution is below 30 ng/mL. World Health Organization (WHO) and US EPA recommend the releasing silver level is under 0.1 mg/L (100 ppb) in drinking water [52]. The releasing rate of silver is below these regulations.

3.2.5. Visual appearance

Silver antimicrobial additives have a great influence on the visual appearance of the coating film. Ag^+ are highly unstable, which can

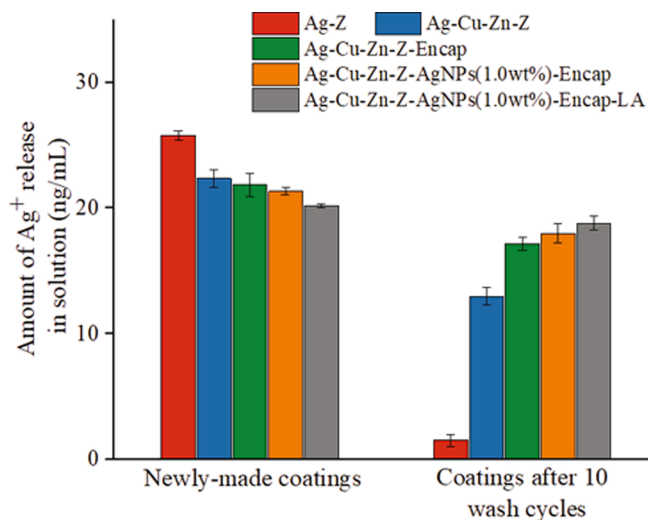


Fig. 14. Silver element analysis by ICP-MS. Silver release from the coating surface by the influence of Na^+ and water. Coatings with high Ag^+ amount left even after ten wash cycles presents long durability.

undergo complex reactions during the curing of powder coatings to form metallic silver, Ag_2O or other silver compounds. The transition of Ag^+ leads to a yellowish appearance, and the smaller the formed silver nanoparticle size, the greater the yellowness. This change is usually uncontrollable, and the final yellowness value cannot be predetermined. Investigating the changes during the curing process is necessary. The curing temperature and time strongly impact the discoloration of antimicrobial coatings, and they are also correlated with the degree of curing.

Fig. 15 performs the relationship between yellowness and degree of curing. When the degree of curing is over 40%, the yellowness goes through rapid growth, so reactions of Ag^+ mainly take place in this range. Meanwhile, the main curing reactions of powder coatings happen within this scope as well. Therefore, the change of film yellowness degree is seriously correlated with the curing reactions. These reactions include ring-opening addition of the epoxy group on TGIC to the acid group and to the hydroxyl group, esterification between the acid and hydroxyl group, and hydrolysis of the epoxy ring by water. The complex and severe reactions promote the reduction of Ag^+ , and due to the narrow space in the zeolite, the formed zerovalent silver is quite fine, resulting in an evident yellowing. Commercial sources of AgNPs normally turns the coatings grey, which mainly influences the brightness of the coating.

The discoloration parameters of samples are shown in Table 3. Ag-Cu-Zn-Z, due to the protection of Cu^{2+} and Zn^{2+} , performs low discoloration change ($\Delta E < 2$). For the AgNPs-containing additives, since the discoloration of commercial AgNPs is known and it will make the surface darker rather than more yellow, which can be compensated by pigment, the discoloration test can be divided into total color change ΔE and change in yellowness Δb . Seen from Table 3, additives 1 and 2 show low ΔE and Δb values because of the low content of silver. Compared to additive 3, additive 4 has a lower value due to the extra protection from the encapsulated polymers to Ag^+ . Although the total color change of additive 10 with the highest silver content reaches a value of 8.26, yellowness changes Δb is only 1.51, showing no evident difference from other additives. Furthermore, the AgNPs leaching out from zeolite will increase ΔE . Thus, the function of LA is evident that ΔE for additive 6 is 7.81, and it is cut down to 6.49 for additive 9, both of which have the same silver loading. Larger ΔE value is shown when increasing the amount of AgNPs, but Δb exhibits little difference.

Besides discoloration, gloss, haze, and distinctness of image (DOI)

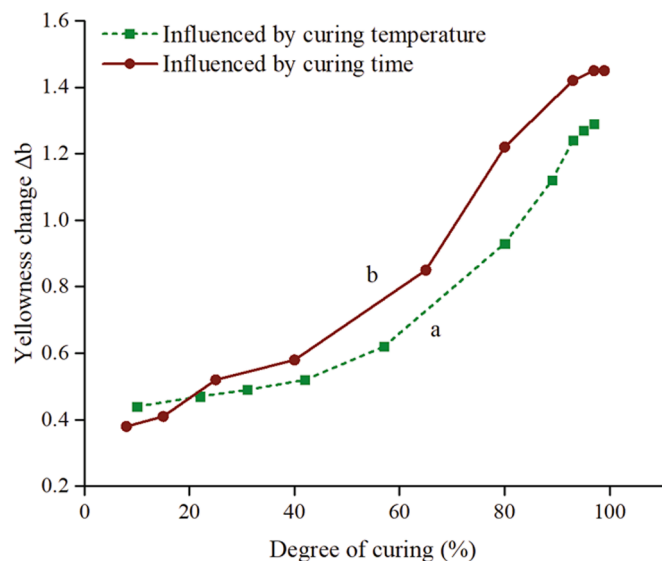


Fig. 15. Relationship between yellowness and degree of curing for Ag-Cu-Zn-Z-AgNPs (1.0 wt%)-Encap-LA additive, influenced by (a) curing temperature (140–220 °C, 10 min) and (b) curing time (200 °C, 1–20 min).

Table 3

Visual appearance measurement of discoloration, gloss, haze, and distinctness of image (DOI) by applying 10 additives into powder coatings.

	Δb	ΔE	Gloss (60°)	Haze	DOI
Control	–	–	94.5	19.5	68.7
Additive 1	0.97	1.12	89.1	24.2	65.7
Additive 2	0.36	0.87	90.7	23.5	63.4
Additive 3	1.37	1.96	88.2	23.6	64.1
Additive 4	1.24	1.47	90.6	25.6	65.8
Additive 5	1.42	5.76	85.6	29.7	56.3
Additive 6	1.49	7.81	82.6	33.6	55.7
Additive 7	1.38	3.98	89.4	26.4	62.5
Additive 8	1.45	5.98	88.1	27.1	60.9
Additive 9	1.43	6.49	87.6	26.5	60.4
Additive 10	1.51	8.26	86.7	31.5	57.2

are important aspects of the visual appearance of powder coating. Micron level of zeolite incorporated in the coating film will cause light refraction and scattering, which may lead to a higher haze value and more “milky” finish. The increased haze value is inevitable when incorporating antimicrobial additives because the size of additive is in micron scale, and these minor inorganic particles existing in clear coat lead to visible blur. However, this change, normally < 5 without AgNPs according to Table 3, is often acceptable in industry. When introducing AgNPs, the haze value raises, and this is because some of the nanoparticles agglomerate outside zeolite particles and form clusters with the size of hundreds of nanometers. These clusters have more influence on the light transmittance, resulting in a high haze. Nonetheless, additives include LA exhibit lower haze value due to its firm bonding ability to AgNPs. It is known that the increase of haze will generally lead to a decrease in gloss. Thus, as shown in Table 3, the gloss value changes in an opposite way to haze. DOI parameter can display a comprehensive evaluation of coating surface quality. Additive 6 with a value of 55.7 suggests the worst appearance due to low gloss and high haze value influenced by the formed clusters of leached-out silver nanoparticles. Similar observations in additives 5 (56.3) and 10 (57.2) can also be attributed to the same cause.

Fig. 16 shows the actual image of the antimicrobial coating on T12G panels. It can be seen that when introducing AgNPs, color change becomes evident. However, when compared to unprotected Ag-Z (8.3 wt %) coating, the color change greatly lessens. Moreover, the color turned slightly darker rather than pure yellowness change (Δb) of the Ag-Z (8.3 wt %) coating. When introducing pigment, color change ΔE can be adjusted to 1.45 (< 2), far lower than the clear coat one (6.49).

To sum up, yellowness change of the coating mainly occurs in the curing process, and the transferred electrons during curing reactions strongly influence the Ag^+ reduction process. AgNPs-incorporated additives have higher ΔE , but acceptable Δb , and the change can be compensated by pigment adjustment. The LA-incorporated one exhibits superiority with minor AgNPs leaching out of zeolite, showing better appearance.

3.2.6. Wettability

Both the ion-exchange and AgNPs oxidation process require a moist environment, so the wettability of the coating surface needs to be determined. Fig. 17 shows the images of the sessile drop and the contact angle readings obtained by the goniometer. The pure polyester/TGIC coating film has a high contact angle of 85.6°, but after incorporating with antimicrobial additives, the contact angles reduce slightly. When treated with Ag-Cu-Zn-Z, the contact angle decreases to 80.4°. Ag-Cu-Zn-Z gives a smaller contact angle value ascribing to the hydration of zeolite. Zeolite can absorb water because of its high specific surface area, and the metal cations in zeolite also grasp water molecules by electrostatic interaction. The encapsulated additives are shown in (c) and (d), exhibiting higher hydrophilicity, with contact angles of 75.5° and 74.2°, respectively. Encapsulated additives comprise many hydroxyl groups,

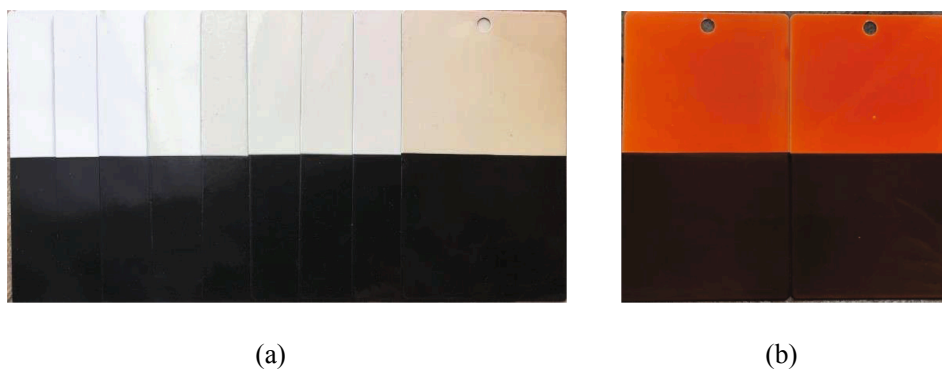


Fig. 16. Images of antimicrobial coatings, (a) clear coat with additives, from left to right: Control, additive 3, additive 4, additive 5, additive 7, additive 8, additive 9, additive 10 and Ag-Z (8.3 wt%); (b) coatings adjusted by orange pigment, left: control, right: additive 9, color change between these coatings: $\Delta E = 1.45$.

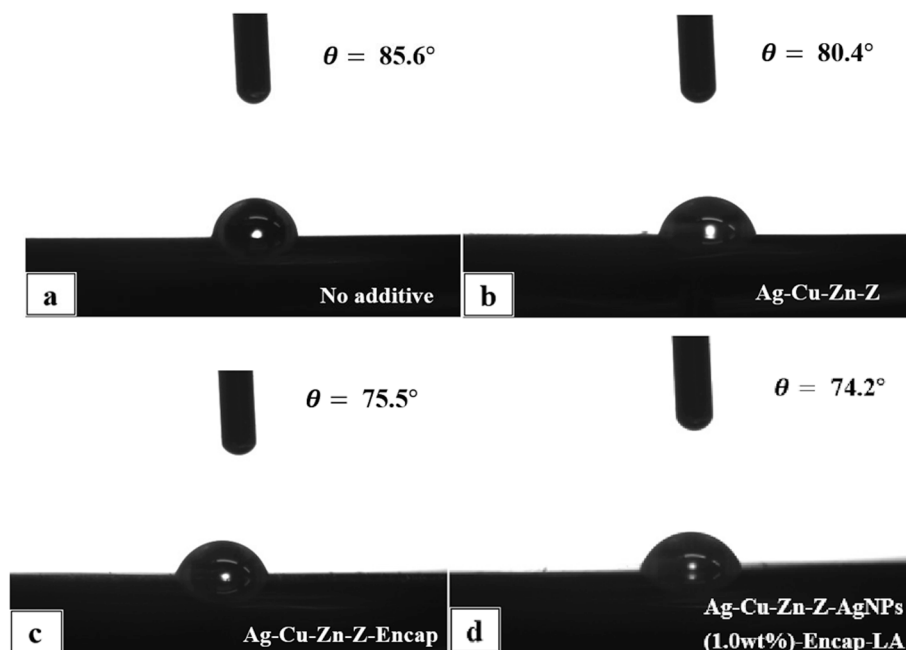


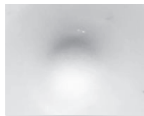

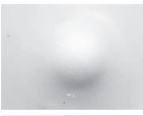







Fig. 17. Contact angle measurement of (a) control, (b) powder coating with Ag-Cu-Zn-Z, (c) powder coating with Ag-Cu-Zn-Z-Encap, and (d) powder coating with Ag-Cu-Zn-Z-AgNPs (1.0 wt%)-Encap-LA by drop shape analysis.

which are beneficial for absorbing water, leading to a smaller contact angle. Moreover, because Ag-Cu-Zn-Z-AgNPs (1.0 wt%)-Encap-LA include lipoic acid, and the zeolite is well-covered by hydrophilic polymers, it shows a smaller contact angle than that of Ag-Cu-Zn-Z-Encap. Enhanced hydrophilicity provokes the release of Ag^+ and strengthens the antimicrobial activity.

3.2.7. Impact test

Incorporating hydrophilic polymers into a powder coating system has some effects on mechanical properties. Table 4 shows the impact test according to ASTM D2794 standard. A standard weight is dropped from a certain distance to strike at the back of the substrate, gradually increasing the distance until visible cracks have been identified. When performing a 40 cm impacting test (392 N·cm), no cracks were

Table 4
Impact test for the four additives according to ASTM D2794 standard.

	No additive	Ag-Cu-Zn-Z	Ag-Cu-Zn-Z-Encap	Ag-Cu-Zn-Z-AgNPs(1.0 wt %)-Encap	Ag-Cu-Zn-Z-AgNPs(1.0 wt %)-Encap-LA
Images and impact strength	 392N·cm	 392N·cm	 392N·cm	 392N·cm	 392N·cm
	 490N·cm	 490N·cm	 490N·cm	 490N·cm	 490N·cm

observed, while at the distance of 50 cm, the coating surface appears cracks, and the encapsulated-additives show a little more cracks. However, the damage of encapsulated-additives coating surfaces is not severe under the same impact strength with 2.0 wt% content of additive.

4. Conclusions

A novel antimicrobial additive was prepared in this work, which contained both Ag⁺ and silver nanoparticles. In this additive, silver nanoparticles were set on an LTA zeolite carrier, and then encapsulated by hydrophilic polymers. These materials were chemically bonded together by α -lipoic acid, so AgNPs were able to be firmly fastened to zeolite and encapsulated inside the hydrophilic polymer. Based on this structure, Ag⁺ was protected inside the zeolite, and the covering AgNPs and hydrophilic polymer reduced their excessive release. The hydrophilic polymer could adsorb water from surroundings to promote AgNPs oxidation, while the synergistic effect of AgNPs and Ag⁺ also accelerated the AgNPs oxidation process, making silver nanoparticles a reservoir of Ag⁺. Therefore, both antimicrobial activity and long durability were ensured.

The prepared additive samples were confirmed by FTIR spectra that the covalent bonds among zeolite, silver nanoparticles, and hydrophilic polymer were formed. The additive particles were heat-stable and could lock water molecules inside zeolite even after the curing process. These additives demonstrated their high efficiency in eliminating widespread microorganisms, including *E. coli*, *S. aureus*, *P. aeruginosa*, and *C. albicans*, and exhibited an over 99.99% efficacy for coatings with exposure of 6 hrs, better than that of commercial sources Zeomic® and Mikrokiller®. Both the wiping test and artificial sweat test results proved excellent durability. Though there was a slight color change of the coating surface that were observed, the yellowness change was acceptable ($\Delta b < 2$), and the brightness change could be compensated by pigment.

Declaration of Competing Interest

The authors declare that they have no known competing financial interests or personal relationships that could have appeared to influence the work reported in this paper.

Acknowledgments

The authors are grateful to the Natural Sciences and Engineering Research Council of Canada (Discovery Grant RGPIN-2018-06256) for supporting this work. The authors also thank the financial support from Guangdong Huajiang Powder Technology Co. LTD.

References

- M. Fernández-Álvarez, F. Velasco, A. Bautista, J. Abenojar, Effect of silica nanoparticles on the curing kinetics and erosion wear of an epoxy powder coating, *J. Mater. Res. Technol.* 9 (1) (2020) 455–464, <https://doi.org/10.1016/j.jmrt.2019.10.073>.
- M. Barletta, A. Gisario, F. Trovati, S. Vesco, Visual appearance and scratch resistance of high performance thermoset and thermoplastic powder coatings, *Prog. Org. Coat.* 76 (1) (2013) 244–256, <https://doi.org/10.1016/j.porgcoat.2012.09.024>.
- J.T. Simpson, S.R. Hunter, T. Aytug, Superhydrophobic materials and coatings: a review, *Rep. Prog. Phys.* 78 (8) (2015) 086501, <https://doi.org/10.1088/0034-4885/78/8/086501>.
- Y. Takeshita, T. Handa, T. Kudo, Improvement of Weathering Resistance for Developed Thermoplastic Polyester Powder Coating for Telecommunication Plant, *ZAKAEP* 59 (6) (2010) 228–231, <https://doi.org/10.3323/jcorr.59.228>.
- Z. Wang, L. Zhang, W. Hu, X. Zhang, G. Zhao, Ultra-heat resistant, adhesive and anticorrosive properties of poly(dimethylsiloxane) resin/furan coating, *Prog. Org. Coat.* 125 (2018) 500–506, <https://doi.org/10.1016/j.porgcoat.2018.10.005>.
- S. Shreepathi, P. Bajaj, B.P. Mallik, Electrochemical impedance spectroscopy investigations of epoxy zinc rich coatings: Role of Zn content on corrosion protection mechanism, *Electrochim. Acta* 55 (2010) 5129–5134.
- Y.H. Wei, L.X. Zhang, W. Ke, Evaluation of corrosion protection of carbon black filled fusion-bonded epoxy coatings on mild steel during exposure to a quiescent 3% NaCl solution, *Corros. Sci.* 49 (2) (2007) 287–302, <https://doi.org/10.1016/j.corsci.2006.06.018>.
- F. Zhang, P. Ju, M. Pan, D. Zhang, Y. Huang, G. Li, X. Li, Self-healing mechanisms in smart protective coatings: A review, *Corros. Sci.* 144 (2018) 74–88, <https://doi.org/10.1016/j.corsci.2018.08.005>.
- B. Shirkavand Hadavand, M. Ataefard, H. Fakhrazadeh Bafghi, Preparation of modified nano ZnO/polyester/TGIC powder coating nanocomposite and evaluation of its antibacterial activity, *Compos. B Eng.* 82 (2015) 190–195.
- L. Dietz, P.F. Horve, D.A. Coil, M. Fretz, J.A. Eisen, K. Van Den Wymelenberg, 2019 Novel Coronavirus (COVID-19) Pandemic: Built Environment Considerations To Reduce Transmission, *mSystems* 5 (2020) e00245-00220.
- D. Cui, X. Liu, P. Hawkey, H. Li, Q. Wang, Z. Mao, J. Sun, Use of and microbial resistance to antibiotics in China: a path to reducing antimicrobial resistance, *J Int Med Res* 45 (2017) 1768–1778.
- Y. Zhou, Y. Deng, P. He, F. Dong, Y. Xia, Y. He, Antibacterial zeolite with a high silver-loading content and excellent antibacterial performance, *RSC Adv.* 4 (10) (2014) 5283, <https://doi.org/10.1039/c3ra44750b>.
- X. Cai, B. Zhang, Y. Liang, J. Zhang, Y. Yan, X. Chen, Z. Wu, H. Liu, S. Wen, S. Tan, T. Wu, Study on the antibacterial mechanism of copper ion- and neodymium ion-modified α -zirconium phosphate with better antibacterial activity and lower cytotoxicity, *Colloids Surf., B* 132 (2015) 281–289, <https://doi.org/10.1016/j.colsurfb.2015.05.027>.
- S. Egger, R.P. Lehmann, M.J. Height, M.J. Loessner, M. Schuppler, Antimicrobial Properties of a Novel Silver-Silica Nanocomposite Material, *AEM* 75 (9) (2009) 2973–2976, <https://doi.org/10.1128/AEM.01658-08>.
- J. Fechner, Jose Zimmer, B. Schultheis, Antimicrobial glass and glass ceramic surfaces and their production, 2007.
- H.J. Johnston, G. Hutchison, F.M. Christensen, S. Peters, S. Hankin, V. Stone, A review of the in vivo and in vitro toxicity of silver and gold particulates: Particle attributes and biological mechanisms responsible for the observed toxicity, *Crit. Rev. Toxicol.* 40 (2010) 328–346.
- D. McShan, P.C. Ray, H. Yu, Molecular toxicity mechanism of nanosilver, *J. Food Drug Anal.* 22 (1) (2014) 116–127, <https://doi.org/10.1016/j.jfda.2014.01.010>.
- J.A. Lemire, J.J. Harrison, R.J. Turner, Antimicrobial activity of metals: mechanisms, molecular targets and applications, *Nat Rev Microbiol* 11 (6) (2013) 371–384, <https://doi.org/10.1038/nrmicro3028>.
- D.M. Mitrano, E. Rimmel, A. Wichser, R. Erni, M. Height, B. Nowack, Presence of Nanoparticles in Wash Water from Conventional Silver and Nano-silver Textiles, *ACS Nano* 8 (7) (2014) 7208–7219, <https://doi.org/10.1021/nn502228w>.
- N. von Goetz, C. Lorenz, L. Windler, B. Nowack, M. Heuberger, K. Hungerbühler, Migration of Ag- and TiO₂-(Nano)particles from Textiles into Artificial Sweat under Physical Stress: Experiments and Exposure Modeling, *Environ. Sci. Technol.* 47 (17) (2013) 9979–9987, <https://doi.org/10.1021/es304329w>.
- L. Budama, B.A. Çakır, Ö. Topel, N. Hoda, A new strategy for producing antibacterial textile surfaces using silver nanoparticles, *Chem. Eng. J.* 228 (2013) 489–495, <https://doi.org/10.1016/j.cej.2013.05.018>.
- J. Cui, R. Yeasmin, Y. Shao, H. Zhang, H. Zhang, J. Zhu, Fabrication of Ag⁺, Cu²⁺, and Zn²⁺ Ternary Ion-Exchanged Zeolite as an Antimicrobial Agent in Powder Coating, *Ind. Eng. Chem. Res.* 59 (2) (2020) 751–762, <https://doi.org/10.1021/acs.iecr.9b05338>.
- R. Yeasmin, H. Zhang, J. Zhu, P. Cadieux, Fabrication and analysis of antimicrobial additives for powder coated surface, *Prog. Org. Coat.* 127 (2019) 308–318, <https://doi.org/10.1016/j.porgcoat.2018.11.016>.
- B. Le Ouay, F. Stellacci, Antibacterial activity of silver nanoparticles: A surface science insight, *Nano Today* 10 (2015) 339–354.
- M.J. Hajipour, K.M. Fromm, A. Akbar Ashkar, D. Jimenez de Aberasturi, I.R. de Larramendi, T. Rojo, V. Serpooshan, W.J. Parak, M. Mahmoudi, Antibacterial properties of nanoparticles, *Trends Biotechnol.* 30 (10) (2012) 499–511, <https://doi.org/10.1016/j.tibtech.2012.06.004>.
- S. Tang, J. Zheng, Antibacterial Activity of Silver Nanoparticles: Structural Effects, *Adv. Healthcare Mater.* 7 (13) (2018) 1701503, <https://doi.org/10.1002/adhm.201701503>.
- J. Liu, R.H. Hurt, Ion Release Kinetics and Particle Persistence in Aqueous Nano-Silver Colloids, *Environ. Sci. Technol.* 44 (6) (2010) 2169–2175, <https://doi.org/10.1021/es9035557>.
- B. Reidy, A. Haase, A. Luch, K.A. Dawson, I. Lynch, Mechanisms of Silver Nanoparticle Release, Transformation and Toxicity: A Critical Review of Current Knowledge and Recommendations for Future Studies and Applications, *Materials (Basel)* 6 (2013) 2295–2350.
- J. Liu, D.A. Sonshine, S. Shervani, R.H. Hurt, Controlled Release of Biologically Active Silver from Nanosilver Surfaces, *ACS Nano* 4 (11) (2010) 6903–6913, <https://doi.org/10.1021/nn102272n>.
- G.A. Sotiriou, S.E. Pratsinis, Antibacterial Activity of Nanosilver Ions and Particles, *Environ. Sci. Technol.* 44 (14) (2010) 5649–5654, <https://doi.org/10.1021/es101072s>.
- B. Liang, E. Jia, X. Yuan, G. Zhang, Z. Su, Salt-responsive polyzwitterion brushes conjugated with silver nanoparticles: Preparation and dual antimicrobial/release properties, *Chem. Eng. J.* 401 (2020), 126114.
- E.A. González, N. Leiva, N. Vejar, M. Sancy, M. Gulppi, M.I. Azócar, G. Gomez, L. Tamayo, X. Zhou, G.E. Thompson, M.A. Páez, Sol-gel coatings doped with encapsulated silver nanoparticles: inhibition of biocorrosion on 2024-T3 aluminum alloy promoted by *Pseudomonas aeruginosa*, *J. Mater. Res. Technol.* 8 (2019) 1809–1818.
- J. Henry, A. Ajaypraveenkumar, G. Sivakumar, K. Mohanraj, A new approach for deposition of silver film from AgCl through successive ionic layer adsorption and

- reaction technique, *J. Cent. South Univ.* 24 (12) (2017) 2793–2798, <https://doi.org/10.1007/s11771-017-3693-4>.
- [34] P. Piszczek, A. Radtke, Silver Nanoparticles Fabricated Using Chemical Vapor Deposition and Atomic Layer Deposition Techniques: Properties, Review, Applications and Perspectives, 2018.
- [35] T. Mokabber, H.T. Cao, N. Norouzi, P. van Rijn, Y.T. Pei, Antimicrobial Electrodeposited Silver-Containing Calcium Phosphate Coatings, *ACS Appl. Mater. Interfaces* 12 (5) (2020) 5531–5541, <https://doi.org/10.1021/acsami.9b20158.s001>.
- [36] H.L. Abd El-Mohdy, Radiation synthesis of nanosilver/poly vinyl alcohol/cellulose acetate/gelatin hydrogels for wound dressing, *J. Polym. Res.* 20 (2013) 177.
- [37] N. Alissawi, V. Zaporozhchenko, T. Strunskus, T. Hrkac, I. Kocabas, B. Erkartal, V.S. K. Chakravadhanula, L. Kienle, G. Grundmeier, D. Garbe-Schönberg, F. Faupel, Tuning of the ion release properties of silver nanoparticles buried under a hydrophobic polymer barrier, *J. Nanopart. Res.* 14 (2012) 928.
- [38] C. Damm, H. Münstedt, Kinetic aspects of the silver ion release from antimicrobial polyamide/silver nanocomposites, *Appl. Phys. A* 91 (3) (2008) 479–486, <https://doi.org/10.1007/s00339-008-4434-1>.
- [39] S. Agnihotri, S. Mukherji, S. Mukherji, Size-controlled silver nanoparticles synthesized over the range 5–100 nm using the same protocol and their antibacterial efficacy, *RSC Adv.* 4 (8) (2014) 3974–3983, <https://doi.org/10.1039/C3RA44507K>.
- [40] D. Paramelle, A. Sadovoy, S. Gorelik, P. Free, J. Hobley, D.G. Fernig, A rapid method to estimate the concentration of citrate capped silver nanoparticles from UV-visible light spectra, *Analyst* 139 (19) (2014) 4855, <https://doi.org/10.1039/C4AN00978A>.
- [41] G.A. Parks, The Isoelectric Points of Solid Oxides, Solid Hydroxides, and Aqueous Hydroxo Complex Systems, *Chem. Rev.* 65 (2) (1965) 177–198, <https://doi.org/10.1021/cr60234a002>.
- [42] K. TEEPARUKSAPUN, N. PRASONGCHAN, A. THAWONSUWAN, Alpha-Lipoic Acid Functionalized Silver Nanoparticles for Colorimetric Detection of Copper Ion, *Anal. Sci.* 35 (4) (2019) 371–377, <https://doi.org/10.2116/analsci.18P442>.
- [43] KUMUDINI CHANDRAKER, SANDEEP.KUMAR. VAISHANAV, REKHA NAGWANSHI, MANMOHAN.L. SATNAMI, Radical Scavenging Efficacy of Thiol Capped Silver Nanoparticles, *J Chem Sci* 127 (12) (2015) 2183–2191, <https://doi.org/10.1007/s12039-015-0968-x>.
- [44] L. Price, K. Leung, A. Sartbaeva, Local and Average Structural Changes in Zeolite A upon Ion Exchange, *Magnetochemistry* 3 (2017).
- [45] B. Kwakye-awuah, D.D. Wemegah, I. Nkrumah, C. Williams, I. Radecka, Antimicrobial Activity of Silver-Zeolite LTA on Heavily-Contaminated Underground Ghanaian Waters, *International Journal of Science and Research* 2 (2013) 26–31.
- [46] P. Wulandari, T. Nagahiro, N. Fukada, Y. Kimura, M. Niwano, K. Tamada, Characterization of citrates on gold and silver nanoparticles, *J. Colloid Interface Sci.* 438 (2015) 244–248, <https://doi.org/10.1016/j.jcis.2014.09.078>.
- [47] G. Huang, M. Wang, Y. Hu, S. Lv, C. Li, Synthesis, characterization, and debromination reactivity of cellulose-stabilized Pd/Fe nanoparticles for 2,2',4,4'-tetrabromodiphenyl ether, *PLoS One* 12 (2017) e0174589.
- [48] J.S. Kirar, S. Khare, Cu(ii) Schiff base complex intercalated into layered double hydroxide for selective oxidation of ethylbenzene under solvent-free conditions, *RSC Adv.* 8 (2018) 18814–18827.
- [49] C. Kosanovic, B. Subotic, I. Smit, A. Cizmek, M. Stubicar, A. Tonejc, Study of structural transformations in potassium-exchanged zeolite A induced by thermal and mechanochemical treatments, *J. Mater. Sci.* 32 (1997) 73–78.
- [50] M. He, Q. Wang, R. Wang, Y.i. Xie, W. Zhao, C. Zhao, Design of Antibacterial Poly (ether sulfone) Membranes via Covalently Attaching Hydrogel Thin Layers Loaded with Ag Nanoparticles, *ACS Appl. Mater. Interfaces* 9 (19) (2017) 15962–15974, <https://doi.org/10.1021/acsami.7b03176.s001>.
- [51] K. Kulthong, S. Srisung, K. Boonpavanitchakul, W. Kangwansupamonkon, R. Maniratanachote, Determination of silver nanoparticle release from antibacterial fabrics into artificial sweat, *Part Fibre Toxicol* 7 (1) (2010) 8, <https://doi.org/10.1186/1743-8977-7-8>.
- [52] P. Dutta, B.o. Wang, Zeolite-supported silver as antimicrobial agents, *Coord. Chem. Rev.* 383 (2019) 1–29, <https://doi.org/10.1016/j.ccr.2018.12.014>.